a substantial lattice energy and consequent low solubility, which accounts for our inability to observe a solution NMR spectrum for this product.

These results confirm a previous report of Schmidbaur[7] concerning gold(III) ylide dimers but also show the chemistry to be much more complicated than originally suggested. Though the source of the extra chlorine atoms in the formation of III'-Cl_4 is uncertain, its formation from II-Cl_2 in the presence of $SnCl_2 \cdot 2H_2O$ is unusual in that an oxidation takes place in the presence of a reducing agent. This reaction opens the path to isomeric gold(III) dimers[18] derived from I.

Acknowledgment. The National Science Foundation (Grant CHE 8408414) and the donors of the Petroleum Research Fund, administered by the American Chemical Society, are thanked for supporting this work. The Robert A. Welch Foundation is acknowledged for supporting some chemical purchases.

Registry No. I (R = Ph), 81457-56-9; II-Cl_2 (R = Ph), 97571-09-0; II-Br_2 (R = Ph), 89462-50-0; III-Br_4 (R = Ph), 98268-94-1; III-$Br_4 \cdot CDCl_3$ (R = Ph), 98391-74-3; III-Cl_4 (R = Ph), 98391-76-5; III'-Cl_4 (R = Ph), 98268-95-2; III'-$Cl_4 \cdot 2CDCl_3$ (R = Ph), 98391-75-4; *trans*,*trans*-$[(Ph_2P(CH_2)_2)_2AuCl_3(CCl_3)]$, 98268-96-3; $[Ph_2P(CH_2)_2AuBr]_2(\mu\text{-}CH_2)$, 90742-64-6; $SnCl_2$, 7772-99-8.

Supplementary Material Available: Listings of thermal parameters, calculated hydrogen atom coordinates, bond lengths and bond angles, and structure factors (Tables V-XII) (28 pages).

Contribution from the School of Chemistry,
University of Western Australia, Nedlands 6009, Australia

Covalent Bonding in *cis*-$[Fe(bpy)_2Cl_2][FeCl_4]$ Studied by X-ray Diffraction at 120 K

B. N. FIGGIS,* P. A. REYNOLDS, and A. H. WHITE

Received January 2, 1985

A valence-orbital-based charge-density analysis of $[Fe(bpy)_2Cl_2][FeCl_4]$ using an extensive accurate X-ray data set collected at 120 K is reported. It complements an earlier spin-density study. Positional and thermal motion parameters agree well with results from neutron diffraction experiments. The crystals form rectangular prisms, with a = 1.4996 (7) nm, b = 1.2325 (7) nm, c = 1.3336 (7) nm, space group *Pccn*, and Z = 8. For the cation we observe for the octahedrally coordinated iron atom valence populations $t_{2g}^{3.42}e_g^{2.04}$, with no significant 4p-like contribution, and "overlap" populations in the Fe–ligand bond centers of 0.06–0.28 e. The chlorine atoms donate substantially to the iron atom (~0.7 e each) while the bipyridyl ligands are *net electron acceptors* (~0.8 e/bipyridyl). There appears to be strong "intermolecular" polarization of the charge distributions on the donor chlorine atoms so that it is not possible to distinguish between σ and π Fe–L bonding contributions with any confidence. The bipyridyl acceptor role is not unexpected since simple theories predict π-back-bonding to be greater than σ-donation. For the anion, the tetrahedrally coordinated iron atom populations are $t_2^{3.94}e^{1.74}$"4p"$^{1.6}$. The chlorine atoms donate substantially to the iron atom, as in the cation about 0.7 e each; again there seems to be strong "intermolecular" polarization of the Cl density, and that inhibits differentiation between σ- and π-bonding. If we compare the metal, donor atom, and bipyridyl charge and spin distributions, both show qualitative features of agreement with simple ligand field and MO treatments of the bonding. However, quantitative incompatibilities of spin and charge result from substantial spin-polarization effects. Thus any quantitative treatment of metal–ligand bonding must allow spin polarization, via for example configuration interaction, to be of more than minor success.

Introduction

The spin and charge distributions in a complex, when combined and compared, give a detailed description of the bonding, as we have shown for the fairly simple molecule, *trans*-tetraammine-dinitronickel(II).[1] We have published a report of a polarized neutron diffraction (pnd) study of the spin distribution in a complex of moderate size, where the data, although lacking in completeness, are of good quality.[2] The complex is *cis*-bis-(2,2'-bipyridyl)dichloroiron(III) tetrachloroferrate(III), Fe-(bpy)Cl_3. We have now obtained an accurate and extensive X-ray data set at a moderately low temperature for Fe(bpy)Cl_3, which we present and discuss in this paper.

The compound Fe(bpy)Cl_3 can be crystallized in the space group *Pccn* with Z = 8.[3] The deuterated material has been studied by using conventional (unpolarized) neutrons to give structures at 4.2 and at 115 K.[4] Both this[3] and another polymorph[5] have been studied by X-ray diffraction at ca. 295 K.

The *Pccn* polymorph is composed of *cis*-$[Fe(bpy)_2Cl_2]^+$ cations and $FeCl_4^-$ anions (Figure 1) each possessing a 2-fold axis, along c. The asymmetric unit consists of half of each of the ions, giving only 25 atoms. The presence of both octahedrally and tetrahedrally coordinated iron(III) in the same unit cell provides the possibilities of a valuable check on consistency and interesting comparisons between the two types of iron atom.

The pnd study[2] showed that over 15% of the spin resides on the donor atoms of the ligands. Surprisingly, little spin appears beyond the nitrogen atoms of the bipyridyl molecules in the ring system. The spin remaining on the two Fe(III) atoms is in each case 3d-like with little evidence of a diffuse (4s-like) component although the possibility of an aspherical 4p-like population could not be excluded. *Qualitatively*, the spin density conforms to simple ligand field theory. We may note that in $Ni(NH_3)_4(NO_2)_2$, also, the pnd experiment yielded results in qualitative agreement with simple ligand theory but that a comparison with the X-ray data showed substantial *quantitative* deviations.

First, using deformation density maps, we shall discuss the qualitative features observed in the charge-density distribution of $[Fe(bpy)_2Cl_2][FeCl_4]$. Quantitative comparison with the pnd results will then be examined by valence population refinements using least-squares methods.

Experimental Section

Partially deuterated (90 (2)%) amber crystals of Fe(bpy)Cl_3 were available.[2] Deuteration helps with the X-ray diffraction studies since at low temperatures the thermal motion is much reduced.[4]

A crystal was mounted on a Syntex $P2_1$ four-circle diffractometer equipped with a locally developed liquid-nitrogen gas-cooled attachment. The cell constants at 120 (3) K were determined by least-squares refinement of the setting angles of six reflections. Monochromatic Mo Kα radiation was employed. A complete sphere of data to 2θ = 30° was collected, accompanied by a hemisphere to 2θ = 80°, with the zero layers $h0l$, $hk0$, and $0kl$, and a further octant to 2θ = 60°. Standard reflection collection, scan widths, and other experimental parameters and corrections were as described previously.[1b] Long-period intensity variations due to equipment instability were about 3%, and any crystal decomposition was undetectable.

Crystal data are given in Table I. After adjustment for variation in the standards, the data were corrected analytically for absorption by using the program ABSCOR of the X-RAY 76 system.[6] The agreement

(1) (a) Figgis, B. N.; Reynolds, P. A.; Mason, R. *J. Am. Chem. Soc.* **1983**, *105*, 440. (b) Figgis, B. N.; Reynolds, P. A.; Wright, S. *J. Am. Chem. Soc.* **1983**, *105*, 434.
(2) Figgis, B. N.; Reynolds, P. A.; Mason, R. *Inorg. Chem.* **1984**, *23*, 1149.
(3) Figgis, B. N.; Patrick, J. M.; Reynolds, P. A.; Skelton, B. W.; White, A. H.; Healy, P. C. *Aust. J. Chem.* **1984**, *36*, 2043.
(4) Figgis, B. N.; Reynolds, P. A.; Lehner, N. *Acta Crystallogr., Sect. B: Struct. Sci.* **1983**, *B39*, 711.
(5) Rieff, W. M., personal communication.

0020-1669/85/1324-3762$01.50/0

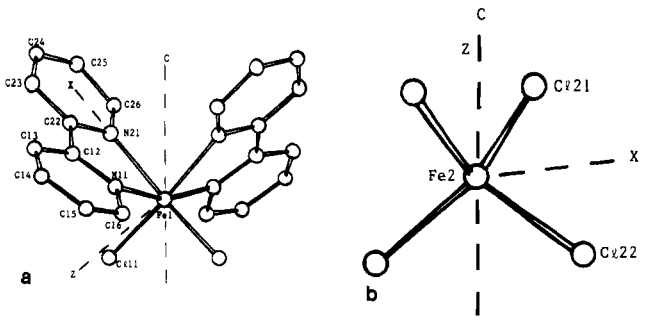

Figure 1. The cation $[Fe(bpy)Cl_2^+]$ and the anion $[FeCl_4^-]$, showing the quantization axes used. Hydrogen atoms are omitted for clarity.

Table I. Crystal Data and Experimental Conditions

temp, K	120 (3)
cryst dimens, mm	0.57 (100) to ($\bar{1}$00)
	0.50 (110) to ($\bar{1}\bar{1}$0)
	0.50 (1$\bar{1}$0) to ($\bar{1}$10)
	0.60 (102) to ($\bar{1}$0$\bar{2}$)
	0.60 ($\bar{1}$02) to (10$\bar{2}$)
space group	*Pccn*
Z	8
unit cell dimens, nm	a = 1.4996 (7)
	b = 1.2325 (7)
	c = 1.3336 (7)
radiation	Mo K$\bar{\alpha}$ ($\bar{\lambda}$ = 71.069 pm)
no. of measd reflcns	52414
no. of avgd reflcns per unique reflcn	5–17
no. of unique reflcns	7696
$(\sin\theta)/\lambda$ max, nm^{-1}	9.05
μ(Mo K$\bar{\alpha}$), mm^{-1}	1.78
transmissn factors	0.445–0.465

factor between equivalents was $R_I = \sum av(|I - av(I)|/\sum av(I) = 0.028$. The standard deviation of each reflection was estimated from the agreement between equivalents, except for very intense reflections where $\sigma(I)/I$ was often <0.01. Because these latter reflections can contain systematic errors, we constrained $\sigma(I)/I$ to be a minimum of 0.0125. The value of $\sum\sigma(I)/\sum I$ that resulted was 0.016.

Models and Results

The Structure and Thermal Parameters. In order to explore bonding effects by using the X-ray diffraction experiment, it is necessary to have an accurate account of the positional and thermal parameters. For comparison with the 295 K results,[3] we performed a refinement (R1) minimizing $\sum(|F_o| - |F_c|)^2/\sigma(F_o)^2$ for data with $I > 3\sigma(I)$. The atomic positional coordinates and thermal parameters (anisotropic for non-hydrogen atoms, isotropic for hydrogen atoms) were refined with the program CRYLSQ in the full-matrix mode as implemented in the X-RAY 76 system.[6] Neutral-atom form factors[7,8] modified for anomalous dispersion[9] were employed. The 5800 3σ data with 179 variables, yielded $R(F) = 0.028$ and $R_w(F) = 0.028$. The 295 K data gave $R(F) = 0.038$ and $R_w(F) = 0.047$ for 1341 "observed" data.[3] The R factors employed here were defined in the usual way.[1b] A less biased refinement is obtained by minimizing the function $\sum\sigma(I_o)^{-2}(I_o - I_c)^2$ and using all the data. Such a refinement (R2) was performed, and yielded for all 7696 data $R(I) = 0.043$ and $R_w(I) = 0.101$.

The low-angle data are more influenced by the valence effects and by the hydrogen atoms. A further refinement (R3) was performed by using only data with $(\sin\theta)/\lambda \geq 4.5$ nm^{-1} and with hydrogen atom parameters fixed at their R2 values. This refinement provides our best estimate of the atomic positional and thermal parameters. A total of 6762 data with 146 parameters yielded $R(I) = 0.049$ and $R_w(I) = 0.099$.

In all the refinements R1–R3 a search for extinction effects yielded negative results.

The R1–R3 positional and thermal parameters are listed in Table II and are compared there with those obtained from a neutron diffraction experiment at 115 K. A scale (120/115) should be applied to the thermal parameters in the latter case to allow for the difference in temperature. The neutron diffraction study was limited in resolution along b, so that U_{22} was too poorly defined to be reported.

Figures 2–5 show X–X deformation density maps. We define the deformation density as $\Delta\rho = \rho_{obsd} - \sum_{atoms}\rho_{spherical}$. The spherical atom density is produced on the assumption of neutral atoms at the positions, given by the high-angle refinement, R3, and with corresponding thermal motions. ρ_{obsd} is calculated from the observed structure factors, after correction for anomalous dispersion, with calculated phases.

Figure 2a and Figure 2c show the deformation density in rings 1 and 2 of the bipyridyl ligand, in the plane obtained by a least-squares fit to the positions of N(11) and C(12) to C(16), and of N(21) and C(22) to C(26) respectively. Figure 3a contains the plane defined by the atoms Fe(1), N(11), and N(21), and Figure 4a contains the plane defined by Fe(1), Cl(11), and Cl(11)′. These planes show the principal features in the cation. Parts a–c of Figure 5 show the deformation density in the anion with three planes respectively containing Fe(2), Cl(21), and Cl(22); Fe(2), Cl(22), and Cl(22)′; and Fe(2), Cl(21), and Cl(21)′.

There are no major peaks not intersected by the above planes: the remainder of the difference density is featureless.

Valence Electron Models. Quantitative estimation of the bonding features was made by using the program ASRED.[1b] Due to the large number of independent atoms and reflections in the present study a full anisotropic refinement of all atoms was not justified. An initial spherical atom valence refinement was made. Subsequently, with all other parameters kept fixed, the atoms in the metal–ligand-bonding region of interest were refined anisotropically (Fe, Cl, and N atoms). The small correlations between all atomic spherical populations indicate that little bias in the anisotropy in the metal–ligand-bonding region should result.

In the spherical refinement the valence electron populations and radial parameters (κ_{atom}) for Fe (3d), C and N (2p), and Cl (3p) were refined individually. At a given scattering wave vector s we use a *valence* form factor $f(\kappa_{atom}|\bar{s}|)$ instead of the theoretical value of $f(|\bar{s}|)$: the core is left unaltered. The valence orbital form factors were the same as used in the previous polarized neutron experiment[2]. Minimizing the function $\sum_{reflections}\sigma^{-2}(I_o)(I_o - I_c)^2$ for 7695 data with 35 variables gives $R(I) = 0.064$, $R_w(I) = 0.080$, χ (goodness of fit) = 2.83. The results are listed in Table IV. The increase in R factors relative to those of R2 follows because of the use of the R3 positional and thermal parameters and is expected as part of our approach.[1b]

The anisotropic refinement requires a choice of quantization axes and hybrid orbitals. Ideally these should constitute a complete set of multipoles for each valence radius. In other cases, involving $\bar{3}$ and $\bar{4}$ site symmetries,[10,11] that formed a manageable problem. In this case, with the ions possessing a 2-fold axis only, a great many parameters (up to 13 per atom) would be required. While the large body of data might support their evaluation, the computation problem would be forbidding and the interpretation of such a parameter set in chemical terms would not necessarily be rewarding. Instead we use a chemically obvious limited basis orbital set, which concentrates on features near the metal atoms where our interest lies. We accept that the goodness of fit to the data will not be fully minimized. We employ five 3d occupation parameters for each iron atom, with axes defined by the local atom environment. Since the iron atoms may not be well described by 3d orbitals alone we also refined 4p populations. On Fe(2) a

(6) Stewart, J. M. "The X-RAY System—Version of 1976", Technical Report TR-446; The Computer Science Center, University of Maryland: College Park, MD, 1976.
(7) Cromer, D. T.; Mann, J. B. *Acta Crystallogr., Sect. A: Cryst. Phys., Diffr., Theor. Gen. Crystallogr.* **1968**, *A24*, 321.
(8) Stewart, R. F.; Davidson, E. R.; Simpson, W. T. *J. Chem. Phys.* **1964**, *42*, 3175.
(9) Cromer, D. T.; Libermann, D. J. *J. Chem. Phys.* **1970**, *53*, 1891.
(10) Figgis, B. N.; Reynolds, P. A. *Inorg. Chem.* **1985**, *24*, 1864.
(11) Figgis, B. N.; Forsyth, J. B.; Mason, R.; Reynolds, P. A. *Chem. Phys. Lett.* **1985**, *115*, 454.

Table IIA. Atomic Positional Coordinates ($\times 10^4$) and Isotropic Thermal Parameters ($Å^2 \times 10^4$)[a]

atom	set	x	y	z	$\bar{U}$	atom	set	x	y	z	$\bar{U}$
Fe(1)	X295	2500	2500	2302.0 (7)	390 (5)	C(23)	X295	345 (4)	4580 (5)	3214 (5)	677 (40)
	R1	2500	2500	2300.3 (2)	146 (1)		R1	326 (1)	4613 (1)	3210 (1)	280 (6)
	R2	2500	2500	2300.1 (1)	98 (1)		R2	325 (1)	4611 (1)	3212 (1)	280 (5)
	R3	2500	2500	2300.1 (1)	141 (1)		R3	323 (1)	4611 (1)	3212 (1)	218 (4)
	N115	2500	2500	2302 (1)	135 (10)		N115	324 (1)	4614 (4)	3213 (2)	238 (20)
Fe(2)	X295	7500	2500	931.3 (8)	596 (7)	C(24)	X295	468 (4)	5529 (5)	2705 (5)	773 (50)
	R1	7500	2500	963.0 (2)	228 (6)		R1	455 (1)	5578 (1)	2700 (1)	316 (7)
	R2	7500	2500	962.9 (1)	227 (1)		R2	454 (1)	5575 (1)	2700 (1)	317 (5)
	R3	7500	2500	963.3 (1)	222 (1)		R3	453 (1)	5580 (1)	2698 (1)	311 (4)
	N115	7500	2500	966 (1)	225 (10)		N115	450 (1)	5577 (5)	2699 (2)	345 (30)
Cl(11)	X295	1582 (1)	1673 (1)	1225 (1)	602 (9)	C(25)	X295	1202 (5)	5660 (4)	2126 (5)	676 (50)
	R1	1580.1 (2)	1660.8 (3)	1202.8 (2)	233 (1)		R1	1207 (1)	5704 (1)	2114 (1)	270 (6)
	R2	1580.2 (2)	1660.5 (2)	1202.8 (2)	234 (1)		R2	1207 (1)	5703 (1)	2113 (1)	270 (5)
	R3	1579.9 (1)	1660.7 (1)	1202.5 (1)	227 (1)		R3	1208 (1)	5707 (1)	2111 (1)	266 (4)
	N115	1580 (1)	1660 (2)	1206 (1)	234 (10)		N115	1206 (1)	5712 (4)	2116 (2)	300 (20)
Cl(21)	X295	8082 (1)	1241 (2)	4 (1)	1073 (20)	C(26)	X295	1797 (4)	4815 (4)	2045 (4)	527 (30)
	R1	8086.7 (3)	1224.6 (4)	12.8 (3)	427 (2)		R1	1806 (1)	4854 (1)	2041 (1)	214 (5)
	R2	8085.8 (2)	1224.6 (3)	12.0 (2)	426 (2)		R2	1805 (1)	4854 (1)	2041 (1)	215 (4)
	R3	8088.2 (2)	1219.9 (3)	16.1 (2)	420 (1)		R3	1808 (1)	4853 (1)	2040 (1)	213 (3)
	N115	8085 (1)	1228 (3)	10 (1)	390 (20)		N115	1804 (1)	4857 (4)	2042 (1)	228 (20)
Cl(22)	X295	6480 (1)	1734 (1)	1844 (1)	713 (10)	H(13)	X295				
	R1	6480.0 (2)	1703.3 (3)	1890.3 (3)	264 (1)		R1	−213 (12)	3008 (15)	4501 (14)	352 (47)
	R2	6479.9 (2)	1703.4 (2)	1890.6 (2)	264 (1)		R2	−252 (9)	3003 (10)	4501 (9)	294 (33)
	R3	6480.1 (1)	1702.9 (2)	1890.9 (2)	259 (1)		R3	−252 (9)	3003 (10)	4501 (9)	294 (33)
	N115	6480 (1)	1704 (3)	1889 (1)	266 (10)		N115	−293 (2)	3076 (6)	4505 (2)	400 (15)
N(11)	X295	1599 (3)	2061 (3)	3495 (3)	453 (20)	H(14)	X295				
	R1	1597 (1)	2062 (1)	3507 (1)	184 (4)		R1	−164 (14)	1397 (17)	5357 (16)	243 (61)
	R2	1597 (1)	2062 (1)	3506 (1)	184 (3)		R2	−165 (10)	1363 (11)	5337 (10)	426 (40)
	R3	1597 (1)	2064 (1)	3507 (1)	181 (2)		R3	−165 (10)	1363 (11)	5337 (10)	426 (40)
	N115	1596 (1)	2064 (2)	3509 (1)	160 (10)		N115	−210	1372 (7)	5467 (2)	390 (16)
N(21)	X295	1681 (3)	3887 (3)	2532 (3)	440 (20)	H(15)	X295				
	R1	1685 (1)	3911 (1)	2529 (1)	177 (4)		R1	1035 (15)	197 (19)	5038 (18)	349 (67)
	R2	1685 (1)	3910 (1)	2529 (1)	177 (3)		R2	1053 (9)	206 (12)	5075 (10)	316 (39)
	R3	1686 (1)	3911 (1)	2528 (1)	173 (2)		R3	1053 (9)	206 (12)	5075 (10)	316 (39)
	N115	1684 (1)	3910 (2)	2529 (1)	169 (10)		N115	1070 (3)	76 (7)	5122 (2)	474 (16)
C(12)	X295	926 (3)	2748 (4)	3673 (4)	457 (30)	H(16)	X295				
	R1	915 (1)	2755 (1)	3680 (1)	195 (5)		R1	2098 (12)	668 (15)	3882 (13)	237 (44)
	R2	914 (1)	2757 (1)	3680 (1)	195 (3)		R2	2117 (8)	668 (10)	3876 (9)	249 (32)
	R3	915 (1)	2755 (1)	3680 (1)	192 (3)		R3	2117 (8)	668 (10)	3876 (9)	249 (32)
	N115	918 (1)	2756 (3)	3682 (1)	155 (10)		N115	2190 (2)	593 (6)	3857 (2)	400 (14)
C(13)	X295	276 (4)	2503 (6)	4353 (5)	670 (30)	H(23)	X295				
	R1	248 (1)	2512 (1)	4367 (1)	279 (5)		R1	−182 (13)	4522 (16)	3603 (15)	329 (55)
	R2	247 (1)	2510 (1)	4368 (1)	278 (4)		R2	−189 (9)	4509 (9)	3569 (9)	294 (33)
	R3	245 (1)	2515 (1)	4368 (1)	275 (4)		R3	−189 (9)	4509 (9)	3569 (9)	294 (33)
	N115	246 (1)	2520 (4)	4369 (2)	220 (20)		N115	−262 (2)	4497 (6)	3680 (3)	411 (15)
C(14)	X295	324 (4)	1558 (6)	4862 (4)	770 (50)	H(24)	X295				
	R1	296 (1)	1547 (1)	4897 (1)	322 (8)		R1	32 (11)	6130 (13)	2757 (12)	357 (38)
	R2	296 (1)	1548 (1)	4898 (1)	322 (6)		R2	28 (9)	6118 (10)	2784 (9)	350 (35)
	R3	293 (1)	1546 (1)	4900 (1)	317 (5)		R3	28 (9)	6118 (10)	3784 (9)	350 (35)
	N115	291 (1)	1550 (4)	4900 (2)	295 (20)		N115	−35 (2)	6235 (8)	2778 (3)	540 (20)
C(15)	X295	1003 (5)	865 (5)	4687 (4)	683 (50)	H(25)	X295				
	R1	993 (1)	846 (1)	4722 (1)	291 (7)		R1	1314 (15)	6319 (18)	1803 (17)	285 (63)
	R2	994 (1)	848 (1)	4723 (1)	286 (5)		R2	1356 (9)	6350 (11)	1770 (10)	351 (35)
	R3	994 (1)	845 (1)	4724 (1)	283 (4)		R3	1356 (9)	6350 (11)	1770 (10)	351 (35)
	N115	995 (1)	841 (4)	4725 (1)	300 (30)		N115	1345 (3)	6456 (7)	1717 (3)	447 (16)
C(16)	X295	1637 (4)	1135 (4)	3993 (4)	563 (30)	H(26)	X295				
	R1	1633 (1)	1129 (1)	4017 (1)	234 (5)		R1	2307 (13)	4903 (16)	1648 (15)	145 (55)
	R2	1635 (1)	1130 (1)	4017 (1)	233 (4)		R2	2321 (7)	4913 (8)	1666 (7)	138 (21)
	R3	1636 (1)	1128 (1)	4017 (1)	230 (3)		R3	2321 (7)	4913 (8)	1666 (7)	138 (21)
	N115	1635 (1)	1126 (4)	4019 (1)	235 (20)		N115	2399 (2)	4920 (7)	1589 (2)	373 (12)
C(22)	X295	967 (3)	3761 (4)	3132 (4)	487 (30)						
	R1	959 (1)	3790 (1)	3124 (1)	195 (5)						
	R2	960 (1)	3791 (1)	3124 (1)	193 (3)						
	R3	959 (1)	3791 (1)	3123 (1)	190 (3)						
	N115	958 (1)	3799 (4)	3125 (1)	160 (10)						

[a] The first entry (X295) is X-ray diffraction at 295 K, followed by R1, R2, and R3 (see text), and the last entry (N115) is the scaled 115 K neutron data. Temperature factors are of the form $T = \exp(-8\pi^2\bar{U}(\sin^2\theta)/\lambda^2)$.

parameter 3d4p—related angularly to the multipole Y_3^{-2}—deals with any noncentrosymmetric density component arising from mixing of 3d and 4p.[12] On the cation we have placed OV(N(1)), OV(N(2)) and OV(Cl) at the Fe–ligand midbonds by using a hydrogen 1s radical dependence to model overlap densities. On the anion the 3d4p parameter performs a similar function.[12] Only the Fe(3d) radial parameters were refined, those for Cl and N being kept unchanged from the previous spherical refinement. Quantization axes and hybrid orbitals used are listed in Table V. The hybrid orbitals $(sp^n)_1$ for the ligand atoms are directed toward the iron atom along local atomic axes x. While this restricted parameter set facilitates interpretation in terms of conventional ligand field theory, it may obscure other interesting, perhaps

(12) Chandler, G. S., Figgis, B. N.; Phillips, R. A.; Reynolds, P. A.; Mason, R.; Williams, G. A. *Proc. R. Soc. London A* **1982**, *384*, 31.

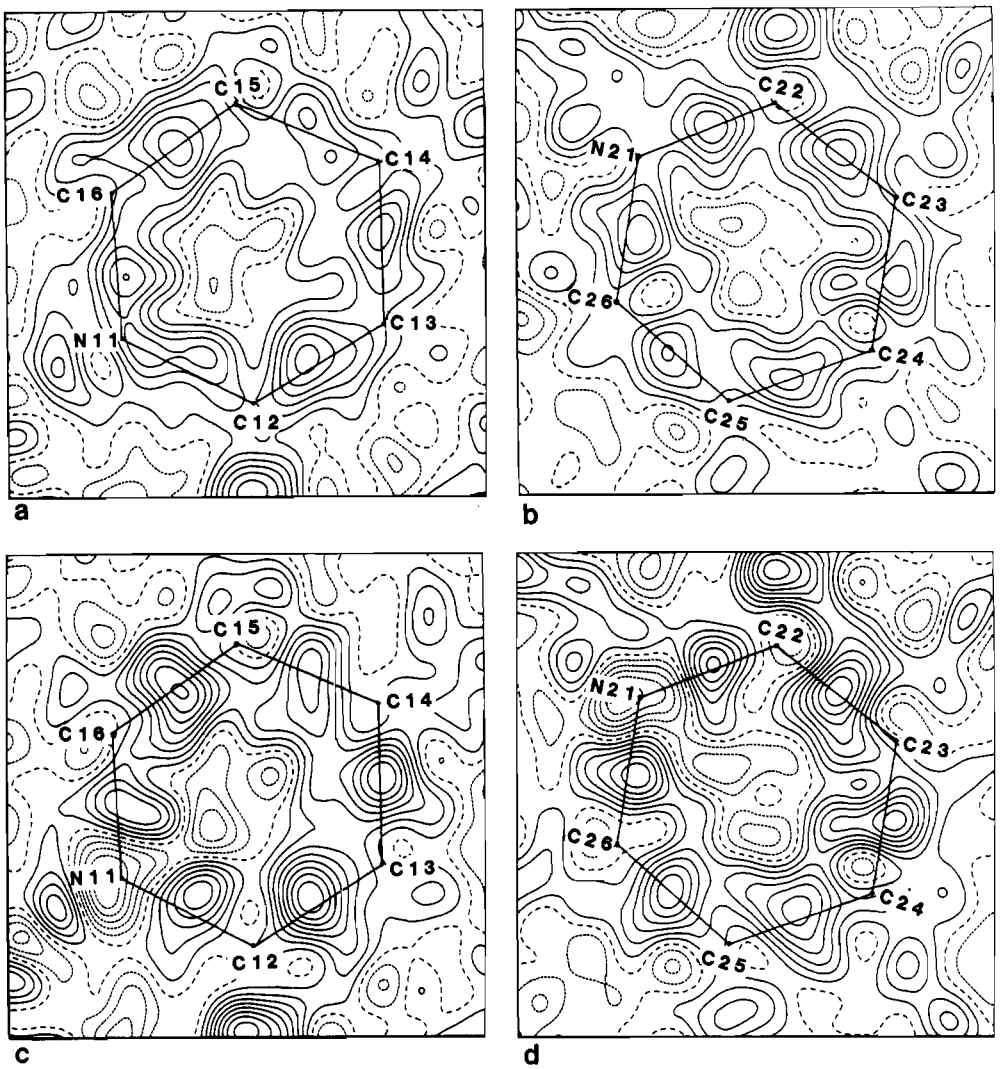

Figure 2. Difference densities in the bipyridyl molecule of the cation (ring 1 = N(11)–(C(12)–C(16)) least-squares plane, ring 2 = N(21)–(C(22) – C(26)) least-squares plane, DD = spherical atom deformation density, RD = valence orbital residual density): (a) ring 1, DD; (b) ring 2, DD; (c) ring 1, RD; (d) ring 2, RD.

Table III. Hydrogen Atom Geometry[a]

Bond Lengths (Å)	
C(13)–H(13)	0.980 (13), 1.075 (2)
C(14)–H(14)	0.935 (14), 1.083 (3)
C(15)–H(15)	0.924 (14), 1.083 (3)
C(16)–H(16)	0.940 (12), 1.079 (2)
C(23)–H(23)	0.915 (13), 1.078 (2)
C(24)–H(24)	0.932 (13), 1.082 (2)
C(25)–H(25)	0.945 (13), 1.077 (2)
C(26)–H(26)	0.924 (10), 1.074 (2)
Bond Angles (deg)	
H(13)–C(13)–C(12)	122.2 (7), 121.5 (2)
H(13)–C(14)–C(14)	119.3 (8), 119.7 (2)
H(14)–C(14)–C(13)	121.5 (9), 119.5 (2)
H(14)–C(14)–C(15)	116.8 (7), 121.7 (2)
H(15)–C(15)–C(14)	121.3 (7), 121.8 (2)
H(15)–C(15)–C(16)	117.6 (8), 118.9 (2)
H(16)–C(16)–N(11)	124.3 (8), 116.9 (2)
H(16)–C(16)–C(15)	116.3 (6), 121.2 (2)
H(23)–C(23)–C(22)	118.7 (7), 121.2 (2)
H(23)–C(23)–C(24)	121.1 (8), 120.0 (2)
H(24)–C(24)–C(23)	119.5 (9), 118.7 (2)
H(24)–C(24)–C(25)	121.1 (7), 122.0 (2)
H(25)–C(25)–C(24)	119.5 (7), 121.7 (2)
H(25)–C(25)–C(26)	123.0 (8), 119.0 (2)
H(26)–C(26)–N(21)	116.9 (8), 116.2 (2)
H(26)–C(26)–N(25)	121.4 (6), 122.2 (2)

[a] In all cases the 120 K X-ray results are given by the first entry, and the 4.2 K neutron results are given by the second.

nonlocal, effects, which will only then appear in the residual density maps.

The 37 variables refined on the 7696 data to give $R(I) = 0.057$, $R_w(I) = 0.075$, and $\chi = 2.66$. The refinement-calculated $F(000)$ of 1291.5 compares well with the formula value of 1277.0. As reasoned previously,[1b] we will use population parameters rescaled by 174/177.69 = 0.979, the ratio of formula and refined valence electron population totals, to provide a best estimate of these latter quantities. They are given in Table VI. As $4p_x$, $4p_y$, and $4p_z$ differ only insignificantly from each other, due to large esd's, only their sum is quoted. Figures 2c,d, 3b, 4b, and 5d–f show the residual densities ($\rho_{obsd} - \rho_{model}$) in the same planes as the previous deformation densities.

Discussion

Structure and Thermal Parameters. We use the previous labeling system for atoms in the structure as shown in Figure 1.[2-4] The 2-fold axis through the iron atoms generates the approximate cis-octahedral stereochemistry about the cation and the near-tetrahedral symmetry of the anion. In the cation, the planes of the pyridyl fragments and Fe(1)–N(11)–N(21) lack coincidence by a few degrees.

The molecular geometry, as defined by the non-hydrogen atoms, does not differ significantly from that determined by neutron diffraction.[4] The hydrogen atom positions, not determined at 295 K,[3] do differ significantly between the X-ray and neutron diffraction studies. The relevant material is presented in Table III. The mean C–H bond is 107.9 (4) pm (neutrons) vs. 93.7 (2) pm (X-rays), with individual bond lengths not differing significantly

Table IV. Results of the Spherical Atom Refinement (Not Valence Rescaled)

(a) Valence Populations (e)

			Anion				
Fe(2) (3d)	5.55 (4)	Fe(2) (4p)	2.0 (3)	Cl(21)	7.33 (6)	Cl(22)	7.42 (6)
			Cation				
Fe(1) (3d)	5.46 (4)	Fe(1) (4p)	0.2 (3)	Cl(11)	7.27 (6)	N(11)	5.55 (5)
N(21)	5.51 (4)						
C(12)	4.03 (3)	C(13)	4.03 (3)	C(14)	4.02 (3)	C(15)	4.02 (3)
C(16)	4.03 (3)	C(22)	4.02 (3)	C(23)	4.04 (3)	C(24)	4.02 (3)
C(25)	4.03 (3)	C(26)	4.01 (3)	H(13)	1.00 (2)	H(14)	1.01 (2)
H(15)	0.99 (2)	H(16)	1.00 (2)	H(23)	1.01 (2)	H(24)	1.01 (2)
H(25)	1.00 (2)	H(26)	1.01 (2)				

(b) Radii (κ)

Fe(2) (3d)	1.062 (4)	Cl(21)	0.984 (4)	Cl(22)	0.986 (4)		
Fe(1) (3d)	1.053 (4)	Cl(11)	0.981 (4)	N(11)	1.013 (5)	N(21)	1.011 (5)

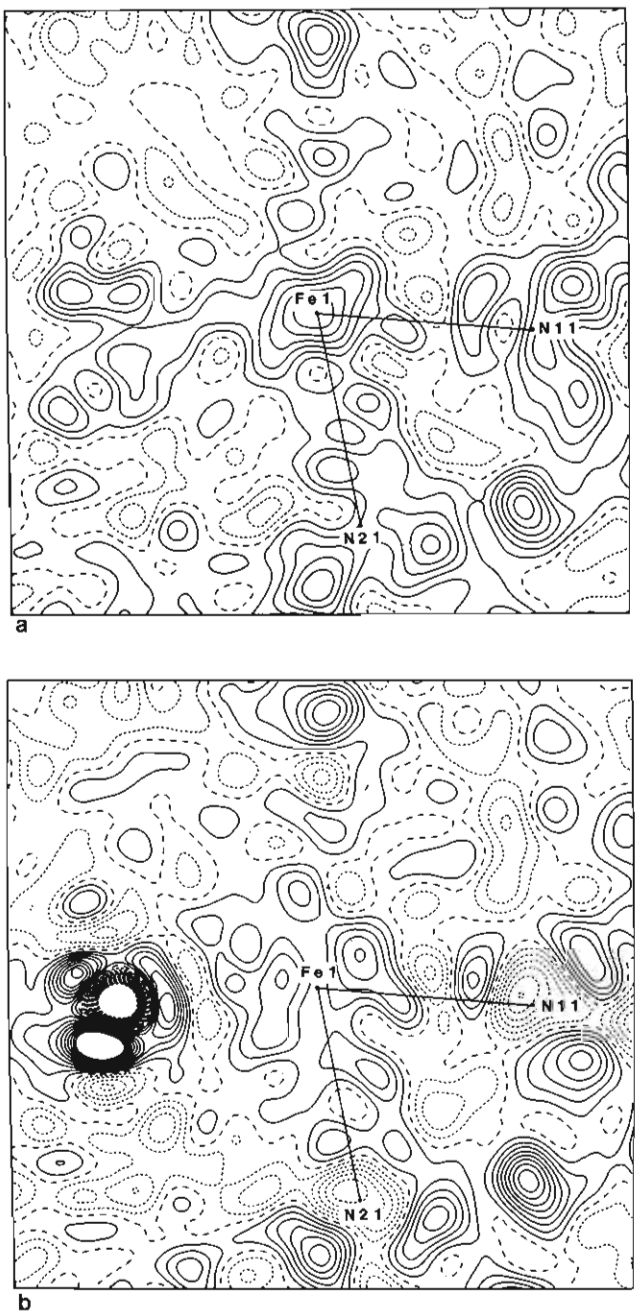

Figure 3. Cation Fe(1)–N(11)–N(21) plane: (a) deformation density; (b) residual density.

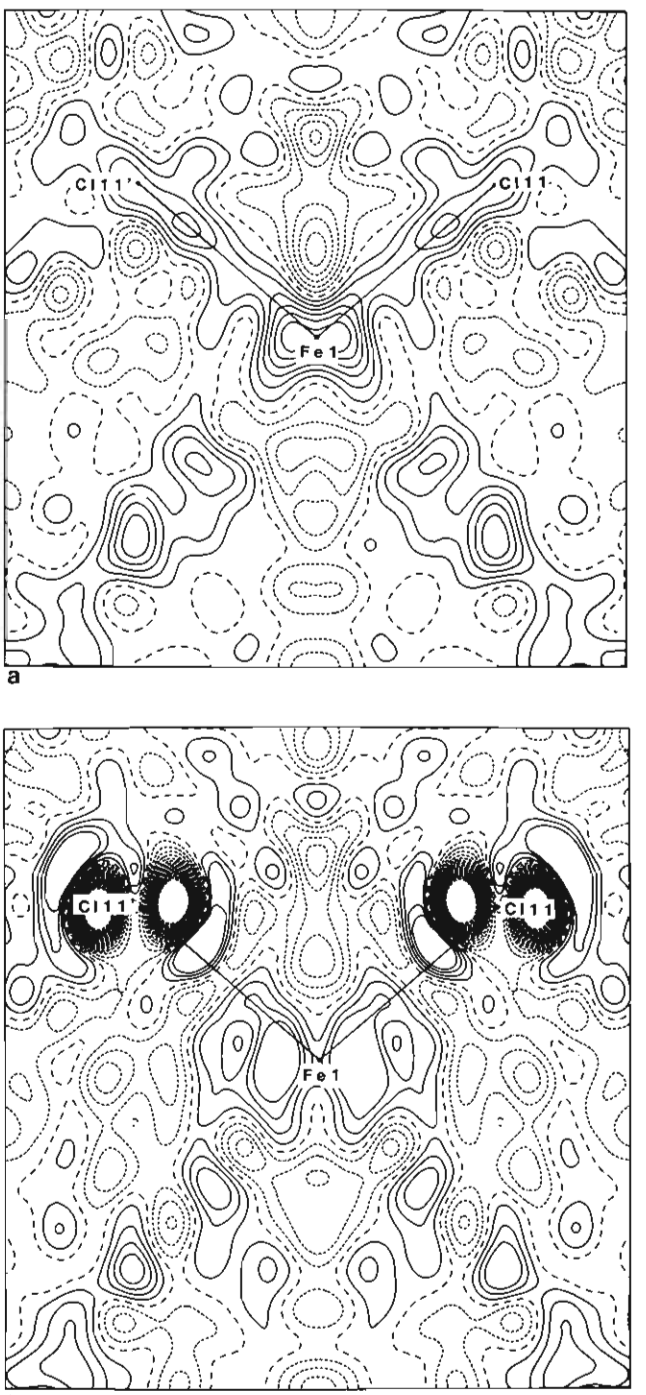

Figure 4. Cation Fe(1)–Cl(11)–Cl(11)′ plane: (a) deformation density; (b) residual density.

from the means. The apparent shortening of bonds to hydrogen atoms in the X-ray structure determinations is well-known.[1a] A more interesting point concerns the bond angles. The neutron

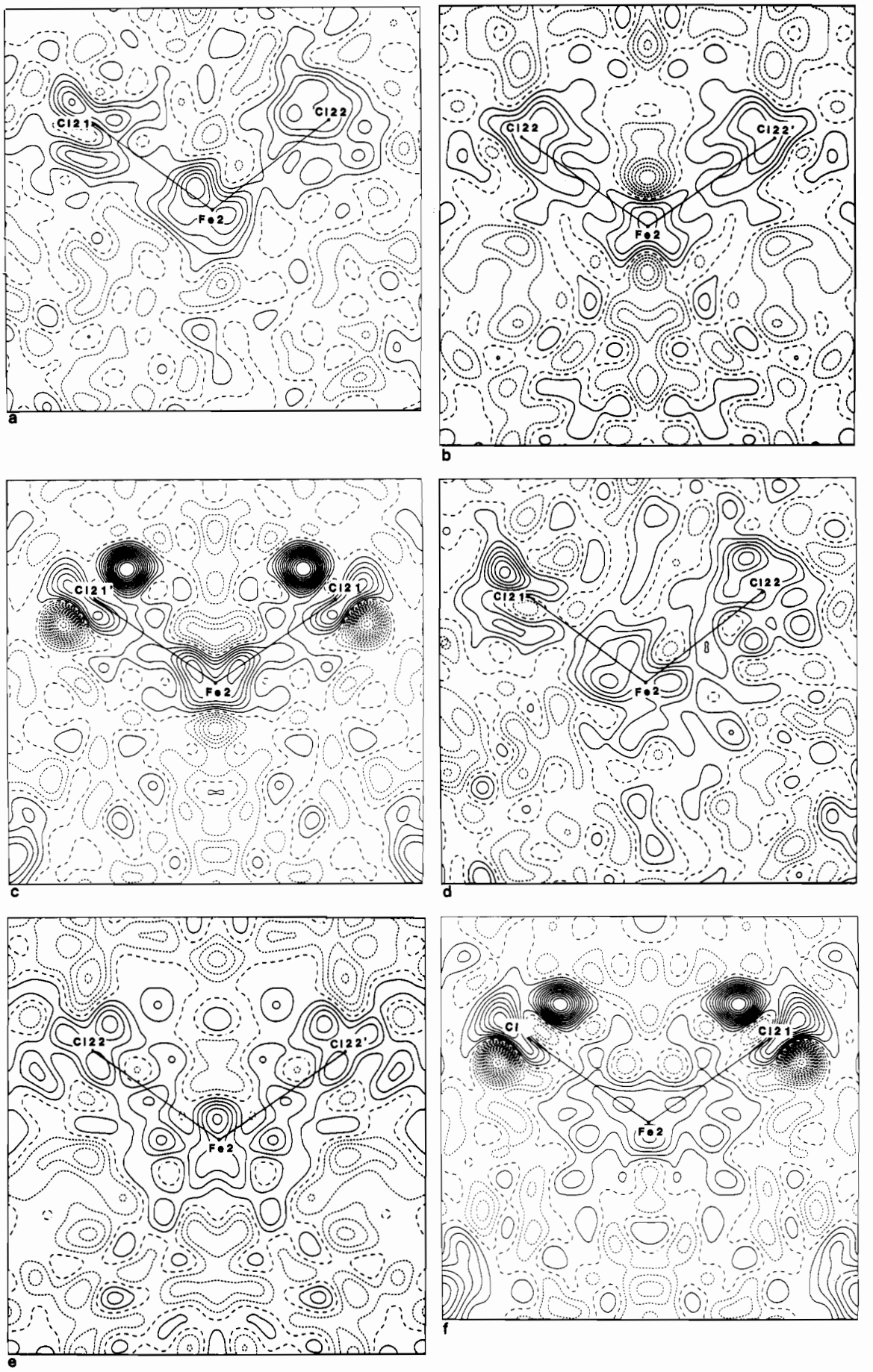

Figure 5. Difference densities in the $[FeCl_4^-]$ anion (P11 = Fe(2)–Cl(21)–Cl(21)′ plane, P21 = Fe(2)–Cl(21)–Cl(22) plane, P22 = Fe(2)–Cl(22)–Cl(22)′ plane, DD = deformation density, RD = residual density): (a) P21, DD; (b) P22, DD; (c) P11, DD; (d) P21, RD; (e) P22, RD; (f) P11, RD.

Table V. Quantization Axes and Hybrid Orbitals Used in the Anisotropic Refinement

atom	z axis	x axis	hybrids
Fe(2)	→c	→(Cl(21) + Cl(22))/2	5×3d, 3×4p, 1×3d4p
Cl(21)	in plane of Fe(2)–Cl(21)–Cl(21)′	→Fe(2)	2×sp, 2×3p$_\pi$
Cl(22)	in plane of Fe(2)–Cl(21)–C6(22)′	→Fe(2)	2×sp, 2×3p$_\pi$
Fe(1)	→N(11)	→Cl(11)	5×3d, 3×4p
Cl(11)	in Cl(11)–Fe(2)–N(11) plane	→Fe(1)	2×sp, 2×sp$_\pi$
N(11)	in plane of ring 1	→Fe(1)	3×sp^2, 1×2p$_\pi$
N(21)	in plane of ring 2	→Fe(1)	3×sp^2, 1×2p$_\pi$
OV(1)			1×"1s"
OV(2)			1×"1s"
OV(3)			1×"1s"

diffraction results show that the C–H bond vectors do *not* bisect the appropriate C–C–C angles and are not predictable from the non-hydrogen atom positions. The angles determined at 120 K by X-ray studies differ on the average by only 2° from the neutron diffraction results. This shows that the apparent bond shortening is caused by a drift of valence electrons from the hydrogen nucleus along the C–H bond vector, as has seen also in the N–H bonds of the $[Co(NH_3)_5(H_2O)]^{3+}$ ion.[13] The C–H bond electronic structure does not seem to vary among the sites in the bipyridyl molecule; the angular distortion of proton position from a C–C–C angle bisector is followed by its associated electron cloud.

The present determination and the 115 K neutron diffraction and the 295 K X-ray studies taken together show no evidence of anharmonicity in atomic motions, and a Debye temperature of 115 K accounts for the thermal motion from 4.2–295 K.[4] Refinements R1–R3 of the present data show no significant changes in the atom positions but show small changes in the thermal parameters, $\overline{U_{ii}}$, decreasing by about 3%.

It is important to establish this lack of anharmonic effects in the present data set, particularly around the iron atoms. We consider the quantity $\sum_k^{\text{atoms}} \sum_{i,j}^{\text{thermal param}} (U_{ij}^{A}(k)/U_{jj}^{B}(k))$. A and B are data sets. These mean ratios should be constant in the high-temperature harmonic approximation and equal to the ratio of the absolute temperatures at which the data sets were obtained. The ratios for the iron, chlorine, and nitrogen atoms are of particular interest. The mean ratio for these atoms for the 120 (3) and 295 (1) K data sets is 0.405 (15); cf. 120/295 = 0.407 (12). The excellent agreement and the small error limits indicate that anharmonic contributions to the thermal motion are quite small. The corresponding ratio for all the carbon atoms is 0.402 (41) supporting the argument within the poorer error limits.

The 120 and 295 K X-ray studies, then, give no significant difference between the derived positional and thermal parameters when scaled for temperature. A much more stringent test is to compare the 115 K neutron and 120 K X-ray diffraction thermal parameters (the positional parameters show no significant differences). We neglect U_{22} since it is poorly defined by the neutron diffraction study.

From the temperatures, we expect the ratio

$$\sum_k^{\text{atoms}} \left| \frac{U_{11}^{X}(k)}{U_{11}^{N}(k)} + \frac{U_{33}^{X}(k)}{U_{33}^{N}(k)} \right|$$

to be 1.04 (4). For the iron, chlorine, and nitrogen atoms the observed ratio is 1.01 (4) and for the carbon atoms 1.01 (6). The maximum value of $|U_{ii}^{X} - U_{ii}^{N}|/(\sigma(Cl_{ii}^{X})^2 + \sigma(U_{ii}^{N})^2)^{1/2}$ is 3.4, and the distribution over i and k appears to be normal. The 120 K X-ray and 115 K neutron diffraction studies therefore show no significant differences in the thermal parameters. This excellent agreement is not usual among such data set comparisons, which have often given X-ray thermal parameters lower than those from neutron diffraction. An example is bis[dicarbonyl(π-cyclopentadienyl)iron(II)], 0.909 (6).[14]

Charge Density—Qualitative Features. We are interested in the change of electron density on bonding, so that the X–X deformation densities of Figures 2a,b, 3a, 4a, 5a, and 6, are sufficient for our purposes. Also, given R3 and the 115 K neutron diffraction agreement, the corresponding X–N maps would not show significant features absent in these maps, except, of course, around the hydrogen atoms.

Parts a and b of Figure 2 show the charge density in the pyridine rings of the bipyridyl molecule and are quite similar. They are as usual for the results of charge density studies on small molecules containing C and N atoms. There is a buildup of charge midway between the non-hydrogen atom bonds; C–C and C–N in the 2,2′-bipyridyl molecule are indistinguishable. In addition, on the bipyridyl molecule, we see at about 65 pm from the nitrogen atoms peaks of height 330 and 310 e nm^{-3}, which we can label "lone pairs". The agreement of the main features in these 2,2′-bipyridyl molecule atoms with those from other experiments on smaller molecules gives confidence in the accuracy of the data set and the reliability of the other maps.

Figure 3a shows that the "lone pairs" mentioned above point directly towards the Fe(1) atom. The features on the other side of this atom are due to a chlorine and to a nitrogen atom in coordination, slightly out of the plane of the diagram. The Fe(1)–Cl(11) bond is illustrated in Figure 4a. As in the Fe(1)–N bonds, we see a bridge of electron density extending between the metal atom and the ligand donor atoms. There is also an excess of charge on the chlorine atoms of σ-symmetry, suggesting that any π-bonding is a good deal less than the σ-bonding.

The density close to the Fe(1) atom is relatively featureless, the peak at this atom not being significant since the errors in X–X maps become large near heavy atoms because of the uncertainty in the scale factor. There is a hole of −500 e nm^{-3} at 80 pm from the iron atom and a depopulation of general nature about 100 pm on each side along the c-axis direction. This feature is suggestive of depletion of a 4p orbital as the distance is larger than expected for 3d orbitals (~60 pm) and it is more diffuse in extent. At 3d distances the density seems almost spherical, as we expect for this formally d^5 ion in octahedral coordination.

For the $FeCl_4^-$ anion, parts a–c of Figure 5 show sections each containing Fe(2) and two chlorine atoms. The Fe^{3+} ion shows a departure from spherical symmetry in the form of a deficit of electron density on both sides along the c-axis direction, here reaching −600 e nm^{-3} at 70 pm. Again there is an excess of density on the chlorine atoms that is connected to the iron atom by a bridge of electron density. The density distribution on the chlorine atoms seems to be rather complex. There is a peak of 1300 and a hole of −1300 e nm^{-3}, both 65 pm from the Cl(21) nucleus and approximately perpendicular to the Fe(2)–Cl(21) bond. This transfer of charge from one side of Cl(21) to the other is by far the strongest feature of the whole deformation density and is not explained by any conventional ligand field theory, since the $FeCl_4^-$ ion is not strongly distorted from tetrahedral. We have examined the short Cl–Cl, Cl–H, and Cl–C nonbonded contacts, which determine the crystal structure, in order to see if the Cl(21) polarization derives from a very close nonbonded contact that fails to change the tetrahedral angles, but none is obvious. There seems to be no simple explanation for the effect, and there is no evidence that it arises from such possible factors as anharmonicity, net electric field gradients, and systematic errors in strong reflections.

Charge Density—Quantitative Features. It appears that many of the features we see in the deformation maps are explicable qualitatively by ligand field models. The valence orbital model will now be used to quantify such features. It will then expose on residual density maps those features inexplicable by simple molecule orbital descriptions of the bonding in such complexes.

Since the spherical and aspherical refinements give similar atomic charges we will quote only the aspherical results. In Table VII we present some charge results obtained by dividing the

(13) (a) Figgis, B. N.; Reynolds, P. A. *Inorg. Chem.* **1985**, *24*, 1864. (b) Figgis, B. N.; Leung, P. C.; Schultz, A. J. *Acta Crystallogr.*, in press.

(14) Mitschler, A.; Rees, B.; Lehmann, M. S. *J. Am. Chem. Soc.* **1978**, *100*, 3390.

Table VI. Anisotropic Valence Refinement Results (Not Valence Rescaled by the Rescaling Factor of 0.979)

(a) Populations

Fe(2)	$3d_{xy}$ = 1.03 (10)	$3d_{yz}$ = 1.24 (8)	$3d_{xz}$ = 1.67 (7)	$3d_{x^2-y^2}$ = 1.24 (10)	$3d_{z^2}$ = 0.50 (8)
Fe(2)	Σ4p = 1.6 (3)	3d4p = 0.9 (9)			
Cl(21)	$(sp)_1$ = 2.23 (5)	$(sp)_2$ = 1.54 (5)	$3p_{\pi z}$ = 1.75 (6)	$3p_{\pi y}$ = 1.96 (6)	
Cl(22)	$(sp)_1$ = 2.20 (5)	$(sp)_2$ = 1.83 (4)	$3p_{\pi z}$ = 1.74 (5)	$3p_{\pi y}$ = 1.80 (5)	
Fe(1)	$3d_{xy}$ = 1.46 (17)	$3d_{yz}$ = 1.02 (17)	$3d_{xz}$ = 0.94 (7)	$3d_{x^2-y^2}$ = 0.88 (11)	$3d_{z^2}$ = 1.16 (10)
Fe(1)	Σ4p = −0.2(3)				
Cl(11)	$(sp)_1$ = 1.43 (5)	$(sp)_2$ = 1.24 (4)	$3p_{\pi z}$ = 2.69 (5)	$3p_{\pi y}$ = 1.86 (5)	
N(11)	$(sp^2)_1$ = 1.46 (3)	$(sp^2)_2$ = 1.34 (3)	$(sp^2)_3$ = 1.57 (3)	$2p_{\pi y}$ = 1.24 (5)	
N(21)	$(sp^2)_1$ = 1.42 (3)	$(sp^2)_2$ = 1.52 (3)	$(sp^2)_3$ = 1.41 (3)	$2p_{\pi y}$ = 1.31 (5)	
OV(N(1))	0.28 (3)				
OV(N(2))	0.06 (3)				
OV(Cl)	0.20 (3)				

(b) Radii (κ)

Fe(2)(3*d*) 1.049 (7) Fe(1)(3*d*) 1.029 (7)

Table VII. Atomic and Fragment Charges (Rescaled)

atom	charge	fragment	charge
Fe(1)	+2.56 (30)	bpy ring 1	−0.29 (8)
Cl(11)	−0.20 (6)	bpy ring 2	−0.45 (8)
N(11)	−0.66 (5)		
N(21)	−0.82 (4)	$Fe(bpy)_2Cl_2$ cation	+0.6 (3)
Fe(2)	+0.83 (30)	$FeCl_4$ anion	−0.6 (3)
Cl(21)	−0.33 (6)		
Cl(22)	−0.41 (6)		

overlap populations equally between bonded atoms ("Mulliken population analysis"). The resulting $FeCl_4$ anion and $Fe(bpy)_2Cl_2$ cation charge of ∓0.6 (3) is in the expected region, between 0 and 1, and gives some confidence in the analysis. Possible systematic errors (for example in the rescaling to the formula $F(000)$) prevent detailed interpretation in terms of cation–anion charge transfer.

(a) $FeCl_4^-$ Anion Results. We have already noted the large polarization of Cl(21), suggesting "intermolecular" effects may be perturbing the system. While the individual valence orbital populations of Cl(21) and Cl(22) show approximate cylindrical symmetry the division between σ- and π-populations differ, indicating that the σ/π-separation may not be clear. The charge transfers of 0.67 (6) and 0.59 (6) e to the iron atom agree, and one would naively expect these to be less affected by external effects than properties described by higher multipoles. Of this total of 2.52 e donated to the iron atom most (1.6 (3) e) seem to end up in diffuse (4p) orbitals, while only 0.66 (4) e is deposited in 3d orbitals. The mean t_2 3d population is 1.28, and the e population is 0.85. The large gain in t_2 with little change in e is consistent with σ-bonding being much stronger than π-bonding. We also notice significant (up to 5σ) departure from cubic symmetry. The assignment of the diffuse density as 4p is supported by the large positive 3d4p mixing coefficient, even though its level of confidence is low.

(b) $Fe(bpy)_2Cl_2^+$ Cation Results. In the cation 0.80 (6) e is transferred from the chlorine atom to the rest of the ion. However *both* pyridyl rings *gain* electrons (0.45 (8) and 0.29 (8) e)! The Fe(1) 4p population remains negligible while the 3d orbitals gain 0.46 e. The Fe(1)–Cl(11) bond appears to be essentially similar to those in the $FeCl_4^-$ anion, in spite of the different geometry and the other ligands. However the *gain* in charge of the bipyridyl molecules indicates that here π-acceptance dominates σ-donation. The two pyridyl rings do not differ appreciably, there being no trace of the cis–trans effect observed in the ionic geometry.[3] Although the errors are large, analysis of the metal 3d population anisotropy suggests a σ-donation of 0.1 (1) e from each pyridyl ring and a π-acceptance of 0.2 (1) e. It does not seem meaningful to separate the chlorine σ- and π-donations. The large residual iron charge of 2.6 (3)+ contrasts with that on Fe(2) in $FeCl_4^-$, the difference arising from the large 4p population in the latter case.

(c) Residual Electron Density. Figures 2c,d, 3b, 4b, and 5d–f show the electron density remaining after subtraction of the valence electron model density from the observed density. In the metal–ligand-bonding region the iron atom densities are noticeably lower, showing the utility of the anisotropic valence model. However, the chlorine atoms still show deep holes and peaks, as Cl(21) did in maps 2–5. We must conclude that the electron densities around the chlorine atoms contain strong polarization features not determined primarily by the Fe–Cl bonds. In general the midbond peaks in the rings are slightly higher, presumably due to correction of the phases of a few weak reflections.

(d) Comparison of Charge- and Spin-Density Results. The spin-density results[2] on $FeCl_4^-$ show a spin transfer of 0.22 (1) to each chlorine with 4.04 (10) 3d and 0.09 4p spins on the Fe^{3+} ion and agree with the charge density in the similarity of the two Fe(2)–Cl bonds. However simple ligand field theory would predict from this spin a *charge* transfer to the iron of 0.22 (1), whereas observation here shows about twice as much, and a negligible 4p population. There is evidence for spin polarization, and that implies the inadequacy of any ligand field or restricted Hartree–Fock type model, for explaining combined spin- and charge-density results. The Fe(2) spin and charge radii (0.989 (9) and 1.062 (7) differ significantly, again possibly because of spin polarization. Spin polarization of formally spin-paired metal-centered orbitals concentrates spin near the Fe nucleus, thus providing a smaller spin than charge radius.

The spin density on the cation shows 4.4 (1) spins in the Fe(1) 3d orbitals with negligible 4p population, 0.23 (2) on each chlorine atom and 0.07 (3) on each bipyridyl moiety. If we average each bipyridyl ring, and further combine C and H populations, we obtain a spin of 0.104 (6) on the nitrogen atom and −0.005 (10) at the ortho, −0.018 (10) and −0.37 (10) at the meta, and +0.015 (10) at the para positions. The negative spin on ortho and meta positions again implies spin polarization. That, together with the much higher populations on nitrogen and carbon para positions can be explained by π-donation of spin into the lowest unoccupied π* pyridine-like orbital which has large N and para but small ortho and meta coefficients. Thus the spin- *and* charge-density results agree that for the bonding to bipyridyl the dominant effect is in π-donation from Fe(3d) to the lowest π* orbitals, while σ-donation to Fe is less significant. Again as for $FeCl_4^-$ the charge transfers are the larger, presumably because of spin-polarization effects. The Fe(1) 3d radii for spin (1.000 (7)) and charge (1.053 (7)) differ, the spin distribution being again less diffuse than the 3d charge distribution.

(e) Comparison with Other Experimental Results and Theory. The much smaller spin transfers than charge transfers observed here are strong evidence for the presence of spin polarization. The negative electron spin on some of the bipyridyl ring carbons is also direct evidence for it, but the statistical significance is weak. We have already observed a similar spin polarization in $Ni(NH_3)_4(NO_2)_2$ when comparing spin and charge densities.[1] These observations have a number of consequences. First, only in relatively simple bonding models, such as ligand field theory, is there any direct theoretical connection between the spin and charge densities. This means that use of spin-density data to determine metal–ligand mixing coefficients in partially occupied single-configuration molecular orbitals is invalid, as is refinement of spin- and charge-density data together to extract single-configuration

molecular orbital bonding parameters. From a theoretical standpoint spin- and charge-density data are equivalent, simple, and fundamental properties—being either sum or difference of up and down spins. It *may* be possible that a restricted Hartree–Fock theory could adequately explain charge-density data alone. However, it certainly cannot explain both spin and charge densities. It would therefore appear mandatory that *any* quantitative bonding theory for transition metals should allow for spin polarization. The two most common such theoretical schemes are either "unrestricted" ab initio or Xα calculations or the introduction of configuration interaction into the ab initio calculations. While such a conclusion is unhelpful in that it further removes bonding from simple LCAOMO explanations, calculations of the types mentioned are now semiroutinely made and are the subject of active research.

Even though quantitatively invalid the use of simple theories, such as the Wolfsberg–Helmholtz model,[15] can qualitatively explain some of the features that we observed in this experiment.

The spin and charge transfers (0.22 and 0.63) observed in the Fe(III)–Cl bond are greater than in the Co(II)–Cl (spin 0.08)[12] and the Ni(II)–Cl bond (charge 0.53).[11] This simple "covalence" order is just that expected by use of spectroscopic data via the spectrochemical series.

While the Fe(III)–Cl bonds appear to be dominated, both in energy and in the densities, by σ-donation, this does not appear so for Fe(III)–bpy bonding. In spectroscopic, i.e. energy-measuring, experiments, the σ-donation from the nitrogen lone pair appears more important than the π-back-donation into the ring π^* orbitals while the converse seems true for the spin and charge densities. This apparent disagreement has already arisen in $Ni(thiourea)_4Cl_2$[11] where the Ni–thiourea and Ni–Cl bond "strengths" appear in different orders in the spectroscopic and diffraction experiments. The same qualitative explanation applies. Energies are more sensitive to metal–ligand overlap integrals, and one would expect the σ-overlap to be larger than the π-overlap, giving the observed dominance of σ-effects in the energies. However spin and charge densities are less sensitive to *overlap*, and, relatively speaking, the *energy difference* between metal orbital and ligand orbital is more important. The π^* orbital is higher in energy than the σ lone-pair orbital and closer in energy to the metal 3d energies. Thus π-back-donation is facilitated and outweighs σ-donation, in spite of the unfavorable overlap, because the orbital energies of metal and ligand (π^*) are better matched.

The large Fe(4p) population in $FeCl_4^-$ and its negligible value in $Fe(bpy)_2Cl_2^+$ may have a qualitative explanation. In earlier work on $Cr(CN)_6^{3-}$,[10] we explain the negligible Cr(III) (4p) populations, while M(II) ions show substantial 4p populations, as due to the larger 3d–4p energy separation in M(III) ions than M(II) ions. However the 3d–4p separation *in a complex* depends not on the formal oxidation state but on what is defined in the Wolfsberg–Helmholtz model as the valence state ionization energies. In $FeCl_4^-$ we see charge donation from *four* chloride ligands reducing the metal "oxidation state". The reduction of the effective oxidation state may be enough to reduce the 3d–4p energy separation so as to allow a significant 4p population to occur. By contrast in $Fe(bpy)_2Cl_2^+$ there are only *two* charge-donating chloride ligands, and the bpy ligands *remove* charge from the metal. The 3d population is thus hardly changed, and the 4p energies remain inaccessible and the orbitals unpopulated.

Lastly we may make the general point, obvious from the residual maps, that *all* atoms are polarized by their neighbors, as well as showing charge transfers. The 3d/4p basis sets on the iron atoms are able to describe the iron polarization well. This is expected since the metal atom is the center of interest, historically, of spectroscopic results for which such basis sets are adequate. Transitions from ligand-centered orbitals have been studied less. Our experiment shows that simple 3s/3p hybridization of the chlorine atoms, with an Fe→Cl quantization axis, may be quite inadequate for describing the polarization of these atoms in the crystal.

Summary

The charge distribution for $[Fe(bpy)_2Cl_2][FeCl_4]$ has been analyzed at a spherical valence electron level for all atoms and also with aspherical distributions in the metal–ligand atom region. All three Fe(III)–Cl bonds show a similar charge transfer, ~0.7 e, to the iron atom, mainly by σ-donation. The two Fe(III)–N bonds are similar and show a charge transfer *to* each pyridyl moiety of ~0.4 e, apparently by π-back-donation from the iron. This unexpected dominance of π-back-donation over σ-donation may be explained by the better energy matching of metal 3d with pyridyl ligand π^* orbitals than with σ-nitrogen lone pairs. The importance of overlap in determining energies renders π-back-donation relatively less important in spectroscopy than in electron density distributions. $Fe(bpy)_2Cl_2^+$ gives the Fe configuration $3d^{5.46}4p^{1.6}$ and respective net charges of +2.6 (3) and +0.8 (3) result. The much larger diffuse ("4p") population, and thus the lower charge on the iron in $FeCl_4^-$, may be due to the smaller 3d–4p energy difference in the $FeCl_4^-$ anion caused by four electron-*donating* chlorides, while two electron-donating chlorides and two electron-*withdrawing* bipyridyls on the cation keep the iron atom "effective oxidation state" in $Fe(bpy)_2Cl_2$ closer to 3. The valence electron anisotropies around the iron and donor atoms, while supporting the preceding description, apparently are also strongly perturbed by intermolecular effects that render more detailed simple ligand field descriptions invalid.

The spin-density results agree in showing σ-donation from chlorine to iron and π-back-donation onto pyridyl π^* orbitals. Thus the qualitative description of bonding in this complex, as determined by spin and charge densities, is as expected, except perhaps for the strength of the "intermolecular" or "long-range" effects. However the spin transfers are much less than predicted from the charge transfers by simple theories. This implies that for *quantitative* explanations theory must be able to deal with spin-polarization effects. Configuration interaction, unrestricted HF–Xα, or other treatments will be required. At a more practical level, attempts to use spin and charge densities to extract individual molecular orbital mixing coefficients for more than a qualitative level of discussion are unjustified.

Acknowledgment. Our thanks are due to the Australian Research Grants Scheme for financial support.

Registry No. *cis*-$[Fe(bpy)_2Cl_2][FeCl_4]$, 88269-35-6.

Supplementary Material Available: Listings of anisotropic thermal parameters (Table IIB) and observed and calculated structure factors for refinement R3 (63 pages). Ordering information is given on any current masthead page.

(15) Wolfsberg, M.; Helmholtz, L. *J. Chem. Phys.* **1952**, *20*, 837.